Measuring the stochastic gravitational-radiation background with laser-interferometric antennas

Nelson Christensen*
Department of Physics, Massachusetts Institute of Technology, Cambridge, Massachusetts 02139
(Received 4 April 1991; revised manuscript received 25 September 1992)

A study of the method of detecting a stochastic gravitation-wave background (SGWB) with laser-interferometric gravitational-wave antennas is presented. The SGWB can be measured by correlating the output of two or more detectors. The results in this paper can be applied to the planned new generation of kilometer length interferometers, such as the Laser Interferometer Gravitational-Wave Observatory (LIGO) in the United States, or similar systems in other countries. Advanced detectors will be able to limit the gravity-wave background energy density per logarithmic interval at 100 Hz to 2×10^{-10} times the closure density of the Universe. A survey of potential sources indicates that a pair of antennas will be able to confirm or deny the existence of cosmic strings, or may detect the background produced by extragalactic neutron star binaries. Elements of the optimal interferometer design and orientation for detecting the SGWB, or any gravity wave, are given. In particular, the criteria for orienting a pair of antennas, the trade-off between sensitivity and bandwidth, and the effect of antenna separation on the correlation are presented. A procedure for obtaining the correlated signal from two interferometers is given. The statistical basis of the correlation experiment is presented. The cause and effect of correlated noise is examined. Filtering and data analysis issues are also discussed.

PACS number(s): 04.80.+z, 04.30.+x, 98.80.Es

I. INTRODUCTION

The construction of kilometer-length laser interferometers to be used to detect gravitational radiation will create a new branch of astronomy. These new antennas will inspect the heavens by detecting the gravitational radiation produced by extremely massive and energetic astrophysical events. Events that are expected to be seen are supernovae, pulsars, and neutron-star binaries. Many groups around the world are working on the design of Michelson delay-line on Fabry-Pérot systems than should eventually achieve a strain sensitivity of $h(f)=10^{-23}/\sqrt{\text{Hz}}$ at 100 Hz [1–3]. The interferometers will operate from the tens of hertz up to about 10 kHz. A review of the current state of gravity-wave research is given by Thorne [3].

Stochastic radiation is considerably different than burst or periodic radiation. It is a background fuzz or a random noise of gravity waves with no evidence of any sharp specific character in either the time or frequency domain. The stochastic gravitational radiation, should it exist, will probably be produced by some cosmological event and would pervade the Universe as a noise on the background metric. The gravity waves are assumed to be stochastic, stationary, and ergodic [4]. They are assumed to be isotropic in that the statical properties can be determined by looking at any section of the sky, just like the microwave background. These gravity waves are completely characterized by their power spectral density.

The SGWB certainly exists at some level and is probably produced by various cosmological events. These events could include phase transitions in the early Universe, quantum fluctuations during inflation, the transition in the Universe's expansion rate from the exponential inflation case to the slower radiation-dominated case, the decay of cosmic strings, or a host of other events. The gravity-wave sources are distributed throughout the Universe, and as the waves interact only very weakly with matter, the background radiation will survive intact. The only change in the character of these cosmologically produced waves will be the redshift due to the expansion of the Universe. The spectrum of the SGWB today will range from frequencies as low as $1/T_{\text{Hubble}}$ to as high as 10^{14} Hz if not higher. Just like the microwave background, the gravity-wave background will be a randomly polarized relic of the early Universe, and its observation will give clues about the history of our cosmos.

The task of detecting the SGWB will be different than for detecting a burst or periodic event. A single detector, be it a laser interferometer or a resonant bar, will be able to register and identify, but not confirm, a burst or a sine wave. This is not the case for the SGWB. The signal recorded by a detector from the SGWB will be indistinguishable from the detector's own intrinsic noise. With a single detector the only certain thing that can be said is that the level of the SGWB signal is less than or equal to the detector's noise level. Unfortunately, there is no way to turn the SGWB on and off to chop the signal. In order to detect the SGWB, one must use at least two detectors and perform a correlation, thereby extracting the common signal from the independent noise of each detector.

The gravity wave detectors measure the unitless strain $h(t)$. The correlation measurement gives the rms value of the strain in the detectors bandwidth, h^2_{rms}, or its spectral density $S_h(f)$, which are related by

*Present address: School of Physics and Astronomy, University of Minnesota, 116 Church St. S.E., Minneapolis, MN 55455.

$$h_{\rm rms}^2=\left\langle \sum_{i,j} h_{ij}h_{ij}\right\rangle = \int_0^\infty df\, S_h(f)\ . \tag{1.1}$$

The gravity-wave spectral density is related to the energy density of this radiation by

$$\rho_{\rm gw}= \int_0^\infty \rho_{\rm gw}(f)df$$
$$= \int_0^\infty \rho_{\rm gw}(\omega)d\omega\ ,\quad \rho_{\rm gw}=S_h(f)\frac{\pi c^2 f^2}{8G}\ . \tag{1.2}$$

The energy density $\rho_{\rm gw}$ is in units of erg/cm^3, while $\rho_{\rm gw}(f)$ is in units of erg/(cm^3 Hz). A useful quantity to express the amount of background gravitational waves is the ratio of the gravity-wave energy density per logarithmic frequency interval to the closure density of the Universe, ρ_c. This ratio $\Omega_{\rm gw}(f)$ is

$$\Omega_{\rm gw}(f)=\frac{1d\rho_{\rm gw}}{\rho_c d\ln f}=\frac{f\rho_{\rm gw}(f)}{\rho_c}\ . \tag{1.3}$$

The value of ρ_c used in this paper is $\rho_c=1.7\times10^{-8}$ erg/cm^3. This assumes that the Hubble constant today is 100 km/(s Mpc).

Some of the hypothesized sources of a SGWB will fall within the operating-frequency band and the range of detectability of the proposed laser interferometers. These events could be the decay of cosmic strings [5], unique equations of state in the very early Universe [6,7], or a background produced by the decay of extragalactic neutron-star binary systems [8] or soliton stars [9]. In the interferometer's operating-frequency band, the cosmic strings may be responsible for a value of $\Omega_{\rm gw}(f)\sim10^{-7}$–$10^{-9}$ [10]. Extragalactic neutron-star binary systems may create a background value of $\Omega_{\rm gw}(f)\sim3\times10^{-10}$ at 100 Hz [8]. The dynamics of the Universe after the Planck time influences the SGWB level. For instance, if the Universe underwent an inflationary expansion phase, the SGWB value today would have a range of possible values of $\Omega_{\rm gw}(f)\sim10^{-17}$–$10^{-22}$ at 100 Hz to 10 kHz [7]. Bubbles created at the end of extended inflation could produce a SGWB with $\Omega_{\rm gw}(f)\sim10^{-5}$ around 1 kHz [11]. If the equation of state for the Universe is $p=-\rho/3$ from the Planck time until 10^{-27} s, then a spectrum with a peak value of $\Omega_{\rm gw}(f)\sim10^{-4}$ at 10 kHz would exist today [12].

This paper addresses how one will measure and quantify the SGWB using laser interferometers. Section II discusses the general transfer functions functions of laser interferometers. In Sec. III a description is given of how one can find the optimum orientation of two interferometers located anywhere on the surface of the Earth. This solution optimizes the detector pair for a search of the SGWB. Section IV contains the explicit analysis for the extraction of the gravity-wave spectrum from the correlated output of two or more interferometers. Section V contains the statistical analysis of the correlation problem and other statistical considerations. Section VI addresses the problem of correlated noise, other than gravitational waves, in both of the interferometers being used for the observation. This is done for a detector pair at the same site and for a pair separated by a continental distance. Section VII is the conclusion.

II. INTERFEROMETER TRANSFER FUNCTIONS

In this section the response of a real laser-interferometer system to a gravitational wave is briefly reviewed. The general transfer for a standard Fabry-Pérot or a Michelson delay line, and for more advanced systems, such as recycling, dual recycling, or resonant recycling, have been presented before [13–18]. The application of these transfer functions to a search for the SGWB is discussed in this section. The optimum bandwidth for a dual-recycling system used in a SGWB search is addressed elsewhere [15].

The gravitational wave is expressed as a Fourier series. If the perturbation to the background metric is real, the gravity wave can be written as

$$h_{ij}(\mathbf{x},t)= \int \frac{d^3\mathbf{k}}{2\eta}\{e^{i(\mathbf{k}\cdot\mathbf{x}-\eta t)}[\tilde{h}_+(\hat{\mathbf{k}},\eta)e_{ij}^+(\hat{\mathbf{k}}) +\tilde{h}_\times(\hat{\mathbf{k}},\eta)e_{ij}^\times(\hat{\mathbf{k}})]+\text{c.c.}\}\ . \tag{2.1}$$

The plus and cross refer to the two polarizations of the gravity wave. The polarization tensors are given as $e_{ij}^+(\hat{\mathbf{k}})$ and $e_{ij}^\times(\hat{\mathbf{k}})$.

The gravity wave is measured by a laser interferometer. What is detected is a change in the intensity of the light coming out the exit port of the interferometer. The signal is proportional to the difference in the phase of the two light beams that recombine at the beam splitter. For a gravity wave with an angular frequency of η, one looks for the output laser light that has had its angular frequency changed from ω to $\omega+\eta$. The definitions have all been carried out with complex quantities and positive frequencies. In a real situation the gravity wave will have a time dependence of $\cos(\eta t+\phi)$ and will produce sidebands on the laser light at the frequencies $\omega\pm\eta$. The lower sideband transfer function can be found by just replacing η with $-\eta$.

As an example, consider a traveling gravity wave coming from a particular part of the sky, with an angular frequency η and a wave vector $\mathbf{k}$, $k=\eta/c$. It has a component h_+ of one polarization and $h_\times$ of the other. The gravity wave is given by

$$h_{ij}=[h_+e_{ij}^+(\hat{\mathbf{k}})+h_\times e_{ij}^\times(\hat{\mathbf{k}})]e^{i(\mathbf{k}\cdot\mathbf{x}-\eta t)}\ . \tag{2.2}$$

The light from the laser that enters the interferometer can be expressed in terms of its electric field, $E_0e^{-i\omega t}$. The interferometers considered operate under a dark-fringe condition. This assumes that under ideal circumstances and in the absence of a gravity wave, there will be no laser light exiting the interferometer in the direction of the photodetector. See Fig. 1 where a delay-line interferometer is illustrated. When there is a gravity wave present, the output electric field at the antisymmetric port photodetector is

$$E_{\rm out}=[h_+S_+(\mathbf{k},\eta)+h_\times S_\times(\mathbf{k},\eta)]E_0e^{-i(\omega+\eta)t}\ . \tag{2.3}$$

The fluctuating intensity of the observed light exiting the interferometer will be due to the gravity-wave-produced sideband beating with a local oscillator field [18]. S_+ and $S_\times$ are the transfer functions for the plus and cross polarizations of the gravity wave with the interferometer. Different optical schemes will be better suited for a measurement of the SGWB than others. The schemes range from broadband detectors, with a frequency range of a few kilohertz, to highly sensitive ones, with an effective bandwidth of only tens of hertz. The transfer functions are general expressions that take into consideration the direction from which the wave is coming and the polarization. General expressions are needed because the SGWB consists of randomly polarized waves from all directions.

A simple delay-line interferometer will be used as an example. Figure 1 illustrates such a system. The light beams in each arm bounce back and forth, traveling a distance of $b \times l$ before exiting. The interferometer will respond to an incoming gravity wave. In the gravity wave's frame of reference, one has

$$g_{\mu\nu}=\eta_{\mu\nu}+h_{\mu\nu}=\eta_{\mu\nu}+h^{(+)}_{\mu\nu}+h^{(\times)}_{\mu\nu} \tag{2.4}$$

and $\mathbf{k}=\{\eta/c\}\times(0,0,1)$. If the gravity wave's coordinate system is represented as (X,Y,Z) and the detector's coordinate system is (x,y,z), then the two systems are related through three Euler rotations, namely,

$$\mathbf{X}=\tilde{R}_z(-\Psi)R_x(\theta)\tilde{R}_z(-\phi)\mathbf{x} \ . \tag{2.5}$$

The relevant components of the metric in the detector's frame are

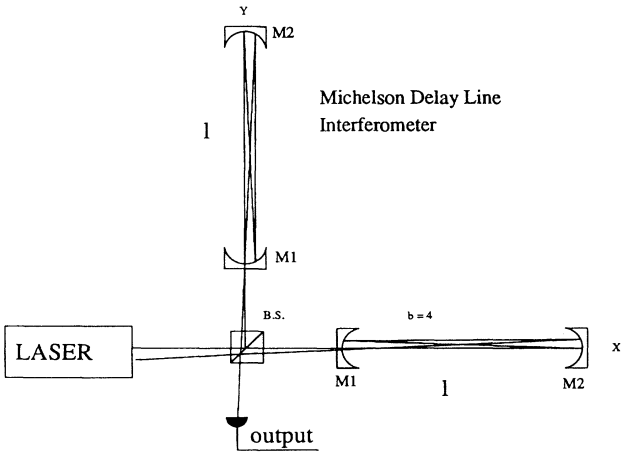

FIG. 1. Example of a delay-line system. Light enters a cavity through a hole in $M1$, traverses the cavity, of length l, a total of b times, and exits through the same hole. The beams from the two cavities recombine at the beam splitter.

$$\begin{aligned} h_{11}&=h_0^{(+)}e^{i(\mathbf{k}\cdot\mathbf{x}-\eta t)}[\cos2\Psi(\cos^2\phi-\cos^2\theta\sin^2\phi)-\sin2\Psi\sin2\phi\cos\theta] \\ &\quad+h_0^{(\times)}e^{i(\mathbf{k}\cdot\mathbf{x}-\eta t)}[\sin2\Psi(\cos^2\phi-\cos^2\theta\sin^2\phi)+\cos2\Psi\sin2\phi\cos\theta] \\ &\equiv[A(\theta,\phi,\Psi)h_0^{(+)}+B(\theta,\phi,\Psi)h_0^{(\times)}]e^{i(\mathbf{k}\cdot\mathbf{x}-\eta t)} \ , \end{aligned} \tag{2.6}$$

$$\begin{aligned} h_{22}&=h_0^{(+)}e^{i(\mathbf{k}\cdot\mathbf{x}-\eta t)}[\cos2\Psi(\sin^2\phi-\cos^2\theta\cos^2\phi)-\sin2\Psi\sin2\phi\cos\theta] \\ &\quad-h_0^{(\times)}e^{i(\mathbf{k}\cdot\mathbf{x}-\eta t)}[\sin2\Psi(\cos^2\phi\cos^2\theta-\sin^2\phi)+\cos2\Psi\sin2\phi\cos\theta] \\ &\equiv[C(\theta,\phi,\Psi)h_0^{(+)}+D(\theta,\phi,\Psi)h_0^{(\times)}]e^{i(\mathbf{k}\cdot\mathbf{x}-\eta t)} \ . \end{aligned} \tag{2.7}$$

In terms of the interferometer's coordinate system, the angles θ and ϕ describe the direction from which the wave came, while Ψ defines the polarization. In terms of the Euler angles defined here, the wave vector in the detector's frame is

$$\mathbf{k}=(\eta/c)(\sin\phi\sin\theta,\ -\cos\phi\sin\theta,\ \cos\theta) \ . \tag{2.8}$$

The Michelson delay-line transfer functions for the two polarizations are

$$\begin{aligned} S_+&=\frac{\pi l}{2\lambda}(1-P_s)R^{(b-2)/2}\sin\left[\frac{\eta lb}{2c}\right]e^{ilb(2\omega+\eta)/2c}(AR_x-CR_y) \ , \\ S_\times&=\frac{\pi l}{2\lambda}(1-P_s)R^{(b-2)/2}\sin\left[\frac{\eta lb}{2c}\right]e^{ilb(2\omega+\eta)/2C}(BR_x-DR_y) \ , \\ R_i&=\left[e^{(il/2c)(ck_i+\eta)}\operatorname{sinc}\left[\frac{1}{2c}(ck_i-\eta)\right]+e^{(il/2c)(ck_i-\eta)}\operatorname{sinc}\left[\frac{1}{2c}(ck_i+\eta)\right]\right]\frac{1}{\sin(\eta l/c)} \ , \end{aligned} \tag{2.9}$$

where λ and ω are the wavelength and angular frequency for the laser beam, R is the reflectivity for the delay line mirrors, P_s is the loss of the beam splitter, and the sinc function is defined as $\operatorname{sinc}(x)=[\sin x]/x$.

The term in the transfer function that depends on the incoming direction and polarization for the wave is AR_x-CR_y for the plus polarization and BR_x-DR_y for the cross polarization. These terms are present in the transfer functions for all interferometer schemes. Their effect is to diminish the transfer function from the ideal

case of $\theta=\phi=\Psi=0$. When this is the case, these terms reduce to $A=1$, $C=-1$, $B=D=0$, and $R_x=R_y=2c/(\eta l)$. It should be noted that R_x and R_y differ very little from the ideal values of $2c/(\eta l)$ over the entire range of the angles θ and ϕ, and over the proposed frequency range of the detectors, from 0 to about 10 kHz. For instance, at 1 kHz, the extreme value of R_x occurs at $\theta=\phi=\pi/2$. The difference between the product $R_x\times\eta l/(2c)$ and one is 3×10^{-4} for a 4-km arm length. The difference is only 0.025 at 10 kHz. The angular-dependent terms enter the problem to an appreciable degree through the terms A, B, C, and D.

The transfer functions for all interferometer schemes (delay line, Fabry-Pérot, recycling, dual recycling, and resonant recycling) can be written in the form

$$\begin{aligned} S_+(\hat{\mathbf{k}},\eta)&=B(\eta)[AR_x-CR_y]\eta l/2c\ , \\ S_\times(\hat{\mathbf{k}},\eta)&=B(\eta)[BR_x-DR_y]\eta l/2c\ . \end{aligned} \tag{2.10}$$

The term $B(\eta)$ is one-half the transfer function for a normally incident and optimally polarized gravity wave. $B(\eta)$ is only dependent on the frequency of the wave and the characteristics of the interferometer. For the purposes of a SGWB detection, one can make the approximation

$$\begin{aligned} S_+(\hat{\mathbf{k}},\eta)&\approx B(\eta)[A-C]\ , \\ S_\times(\hat{\mathbf{k}},\eta)&\approx B(\eta)[B-D]\ . \end{aligned} \tag{2.11}$$

III. INTERFEROMETER ORIENTATION

In this section the optimum orientations of two laser interferometers in search of the SGWB are derived [19]. These antennas are situated at different locations on the surface of the Earth. The two arms of an interferometer are assumed to be perpendicular to each other and of equal length.

A. Coordinate system

The coordinate systems that are used to express the response of a detector to an incoming wave are described first. The coordinates (X,Y,Z) will be associated with the incoming gravity wave. The coordinates (x,y,z) will be fixed with respect to the Earth. If one were at the north pole, the $\hat{\mathbf{x}}$ direction would point along the Greenwich mean line, 0° longitude. The $\hat{\mathbf{y}}$ direction points along the 90°E longitude line. The $\hat{\mathbf{z}}$ direction is perpendicular to the surface of the Earth at the north pole. Finally, (x_1,y_1,z_1), and (x_2,y_2,z_2) refer to the local coordinate systems of our two detectors.

The coordinate systems are related to each other by series of Euler rotations. The rotations and coordinate systems are defined to be

$$\begin{aligned} \mathbf{X}&=\tilde{R}_z(-\Psi)\tilde{R}_x(\theta)\tilde{R}_z(-\phi)\mathbf{x}\ , \\ \mathbf{x}_1&=\tilde{R}_z(g_1)\tilde{R}_x(b_1)\tilde{R}_z(a_1)\mathbf{x}\ . \end{aligned} \tag{3.1}$$

The angles θ and ϕ define the direction from which the gravity wave is coming. The angle Ψ defines the polarization of the wave. The angles a_1 and b_1 define the location of detector one on the Earth. Specifically, $a_1=\gamma_E-3\pi/2$ and $b_1=\pi/2-\beta_N$, where γ_E is east longitude value and β_N is the north latitude value. The variable g_1 represents the angle between the local east-west line and the interferometer arm that defines its $\hat{\mathbf{x}}$ axis. The $\hat{\mathbf{x}}$ arm is uniquely defined if one demands that the $\hat{\mathbf{z}}$ point radially out from the Earth at the detector and that one has a right-hand coordinate system. See Fig. 2.

Let us assume that a gravity-wave interferometer has its arms along the $\hat{\mathbf{x}}$ and $\hat{\mathbf{y}}$ axes of the Earth-centered coordinate system. The gravity-wave interferometer would measure a signal with an amplitude of

$$h=\tfrac{1}{2}(h_{11}-h_{22})\ , \tag{3.2}$$

$$\begin{aligned} h_{11}&=A(\theta,\phi,\Psi)h_0^{(+)}+B(\theta,\phi,\Psi)h_0^{(\times)}\ , \\ h_{22}&=C(\theta,\phi,\Psi)h_0^{(+)}+D(\theta,\phi,\Psi)h_0^{(\times)}\ , \end{aligned} \tag{3.3}$$

and so

$$\begin{aligned} h&=\tfrac{1}{2}[h_0^{(+)}(A-B)+h_0^{(\times)}(C-D)] \\ &=h_0^{(+)}F_+ +h_0^{(\times)}F_\times\ , \end{aligned} \tag{3.4}$$

$$\begin{aligned} F_+&=\tfrac{1}{2}(1+\cos^2\theta)\cos2\phi\cos2\Psi-\cos\theta\sin2\phi\sin2\Psi\ , \\ F_\times&=\tfrac{1}{2}(1+\cos^2\theta)\cos2\phi\sin2\Psi-\cos\theta\sin2\phi\cos2\Psi\ . \end{aligned} \tag{3.5}$$

When a detector is located at some general location on the Earth, F_+ and $F_\times$ become very long and cumbersome. They are a function of the six Euler angles θ ϕ, Ψ, a, b, and g. Detector 1 would measure a strain

$$\begin{aligned} h&=\tfrac{1}{2}(h_{11}-h_{22})=\tfrac{1}{2}[h_0^{(+)}(A_1-B_1)+h_0^{(\times)}(C_1-D_1)] \\ &=h_0^{(+)}F_{1+}(\theta,\phi,\Psi,a_1,b_1,g_1) \\ &\quad +h_0^{(\times)}F_{1\times}(\theta,\phi,\Psi,a_1,b_1,g_1)\ . \end{aligned} \tag{3.6}$$

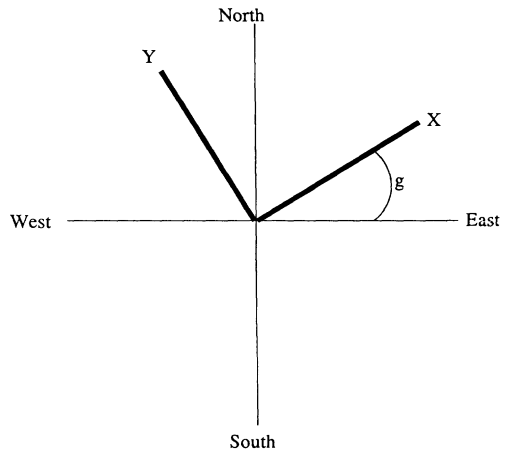

FIG. 2. This displays the interferometer, in bold, in relation to its local longitude and latitude lines. The angle g represents the angle between the local east-west line and the interferometer arm that defines its $\hat{\mathbf{x}}$ axis.

B. Solution for the optimum orientation

The optimum orientation of two detectors is found by locating extrema in the correlated output of these two antennas in an isotropic, stochastic background of gravitational radiation. In other words, given the location of the two detectors, specified by (a_1,b_1), and (a_2,b_2), one must find the values of g_1 and g_2 that correspond with the extrema of

$$\int_0^{2\pi} d\phi \int_0^{\pi} \sin\theta \, d\theta (F_{1+}F_{2+}+F_{1\times}F_{2\times}) \, . \tag{3.7}$$

This will then yield the best correlation measurement. There is no $F_+F_\times$ cross term because the correlation between the two polarizations of a stochastic and randomly polarized background vanishes. Furthermore, the correlation is independent of the polarization angle Ψ, thereby simplifying the calculation, as one may now set Ψ equal to zero. This is equivalent to averaging over the angle Ψ. A rotation of 90° about the detector's $\hat{\mathbf{z}}$ axis does not change the amplitude of the response of an interferometric gravity-wave antenna. Sometimes the extrema of Eq. (3.7) are found for the situation where the orientation of one of the detectors is fixed, as certain detector sites only allow a particular orientation. To be perfectly general, an extrema should be found for the equation

$$\int_0^{2\pi} d\phi \int_0^{\pi} \sin\theta \, d\theta (F_{1+}F_{2+}+F_{1\times}F_{2\times})\cos\mathbf{k}\cdot\mathbf{x} \, , \tag{3.8}$$

where $\mathbf{k}$ is the gravity wave's wave vector and $\mathbf{x}$ is the vector from the center of detector 1 to the center of detector 2. However, inclusion of the cosine term does not significantly change the results. In fact, finding the extrema to Eq. (3.7) is the best strategy for detecting the SGWB. This point will be discussed further in Sec. IV.

There is a nice physical picture for the optimum orientation of two interferometric detectors. When one finds values of g_1 and g_2 that correspond with an extrema for Eq. (3.7), one has the physical situation where one arm of each interferometer points along the great circle that connects the centers of each interferometer, while the other arms are parallel to each other. Using this method, one can easily find the optimum orientation of two detectors located at different points on the Earth. The great circle connecting the two sites defines a nice coordinate system that makes the solution to Eq. (3.7) trivial. Consider the scenario where $a_1=b_1=g_1=0$ and $a_2=a$, $b_2=g_2=g$. The solution to Eq. (3.7), normalized to the case where the two interferometers are aligned at the same location, is

$$\begin{aligned} S_A &= \frac{5}{8\pi} \int_0^{2\pi} d\phi \int_0^{\pi} \sin\theta \, d\theta (F_{1+}F_{2+}+F_{1\times}F_{2\times}) \\ &= \tfrac{1}{2}(1+\cos^2 b)\cos 2a \cos 2g - \cos b \sin 2a \sin 2g \, . \end{aligned} \tag{3.9}$$

Call the angle between the $\hat{\mathbf{x}}$ arm of detector 1 and the great circle η_1 and the angle between the $\hat{\mathbf{x}}$ arm of detector 2 and the great circle η_2. Also, call the angle between the interferometer bisector of detector 1 and the great circle Ψ_1 and the angle between the interferometer bisector of detector 2 and the great circle Ψ_2 (see Fig. 3). The solution S_A given above can be expressed in terms of these angles. One needs to make the substitutions $\eta_1=a$, $\Psi_1=a+\pi/4$, $\eta_2=g-\pi/2$, and $\Psi_2=g-\pi/4$. The result is

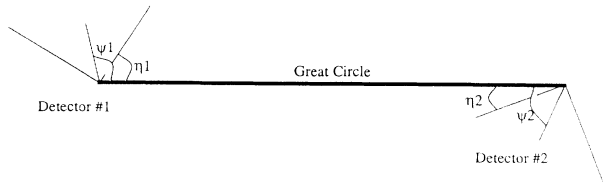

FIG. 3. Definition of the angles for the two detectors with respect to the great circle. The angle η is between the great circle and the $\hat{\mathbf{x}}$ arm of the detector, while Ψ is between the great circle and the interferometer's bisector.

$$\begin{aligned} S_A &= -\tfrac{1}{2}(1+\cos^2 b)\cos 2\eta_1 \cos 2\eta_2 + \cos b \sin 2\eta_1 \sin 2\eta_2 \\ &= -\tfrac{1}{2}(1+\cos^2 b)\sin 2\Psi_1 \sin 2\Psi_2 + \cos b \cos 2\Psi_1 \cos 2\Psi_2 \, . \end{aligned} \tag{3.10}$$

When both interferometers have the optimum alignment, with each having one arm point along the great circle connecting the two locations, then the solution for S_A depends only on the angle of arc around the Earth between them. This angle β is given by

$$\beta = \arccos[\cos b_1 \cos b_2 + \sin b_1 \sin b_2 \cos(a_1 - a_2)] \, . \tag{3.11}$$

The normalized general solution is

$$S_A = \tfrac{1}{2}(1+\cos^2\beta) \, . \tag{3.12}$$

The relative orientation to optimize the detection of a SGWB is the same as for the coincident detection of gravitational wave bursts but the reduction in coincidence sensitivity in a burst search with misalignment is gentler [20].

IV. CORRELATION EXPERIMENT

This section presents the general solution for the correlation of the output of two arbitrary interferometric gravitational-radiation antennas and how it is to be related to a SGWB. The solution is general in that the individual interferometers can have any transfer function, they can be located at any site on the surface of the Earth, they can have any orientation at these sites, and their intrinsic noise spectral density may take any shape.

A. Stochastic gravitational-wave background

The gravitational-radiation background expressed as a Fourier transform is given by Eq. (2.1). The $\tilde{h}$ terms are the Fourier transforms of $h_{ij}(\mathbf{x},t)$ for each polarization. They are assumed to be stochastic random variables. Also, it is assumed that the component $h_+(\hat{\mathbf{k}},\eta)$ is uncorrelated with any other $h_+(\hat{\mathbf{k}}',\eta')$, unless $\mathbf{k}=\mathbf{k}'$. We can express this formally as

$$\begin{aligned} \langle \tilde{h}_+(\hat{\mathbf{k}},\eta)\tilde{h}_+(\hat{\mathbf{k}}',\eta')\rangle &= \langle \tilde{h}_\times(\hat{\mathbf{k}},\eta)\tilde{h}_x(\hat{\mathbf{k}}',\eta')\rangle \\ &= |\tilde{h}_0(\eta)|^2 \delta^{(3)}(\mathbf{k}-\mathbf{k}') \, . \end{aligned} \tag{4.1}$$

The magnitudes of the two polarization terms are the same. It was assumed here that the background is isotropic. It is also assumed that for a given $\hat{\mathbf{k}}$ the two polarization states are uncorrelated. The background is randomly polarized, which can be expressed as

$$\langle \tilde{h}_+(\hat{\mathbf{k}},\eta)\tilde{h}_\times(\hat{\mathbf{k}},\eta)\rangle = 0 \ . \tag{4.2}$$

B. Measurable quantities

The first measurable quantity to consider is the output of the interferometric gravity-wave antenna. What is detected is the change in the intensity of the output laser light due to a phase difference of the light in each arm of the interferometer. When a traveling gravity wave of angular frequency η passes through the interferometer, a beam of laser light with components of angular frequency $\eta+\omega$ and $\eta-\omega$, where ω is the angular frequency of the input laser light, will be produced. The measurable quantity will be the fluctuating intensity of the sideband beating with a reference local oscillator field [18]. The real-valued output of interferometer 1 at time t and location $\mathbf{x}_1$, due to the gravity wave $h_{ij}(\mathbf{x},t)$, is

$$z_1(t) = \int \frac{d^3\mathbf{k}}{2\eta}\left[e^{i(\mathbf{k}\cdot\mathbf{x}-\eta t)}\{\tilde{h}_+(\hat{\mathbf{k}},\eta)S_+(\hat{\mathbf{k}},\eta)+\tilde{h}_\times(\hat{\mathbf{k}},\eta)S_\times(\hat{\mathbf{k}},\eta)\}+\text{c.c.}\right] . \tag{4.3}$$

One can now express the correlation of the output to two gravity-wave interferometers located at $\mathbf{x}_1$ and $\mathbf{x}_2$, with a time delay τ as

$$\begin{aligned}\langle z_1(t)z_2(t+\tau)\rangle = \int_0^\infty \frac{d\eta\, G\rho_g(\eta)}{c^2\eta^2}\int_0^{2\pi} d\phi \int_0^\pi \sin\theta\, d\theta \Bigg[e^{i[\mathbf{k}\cdot(\mathbf{x}_1-\mathbf{x}_2)+\eta\tau)]} \\ \times \left[\frac{\eta}{2c}\right]^2 l_1 l_2 \{(A_1R_{x1}-C_1R_{y1})(A_2R_{x2}^*-C_2R_{y2}^*)B_1(\eta)B_2^*(\eta) \\ +(B_1R_{x1}-D_1R_{y1})(B_2R_{x2}^*-D_2R_{y2}^*)B_1(\eta) \\ \times B_2^*(\eta)\}+\text{c.c.}\Bigg] ,\end{aligned} \tag{4.4}$$

where the transfer function term $B(\eta)$ was defined in Sec. II. Equation (4.4) is the general expression. All of the quantities in the expression for $\langle z_1 z_2\rangle_{\text{av}}$ will be known, except for the size and spectrum of the SGWB.

The expression for $\langle z_1 z_2\rangle_{\text{av}}$ can be simplified by noting that, for the range of frequencies in which the currently planned long-baseline interferometers will be operating, the terms $R_i\eta l/(2c)$ are virtually constant at one. Also, the LIGO system is to be built with identical interferometers at each antenna location. In this case the correlation reduces to

$$\begin{aligned}&\langle z_1(t)z_2(t+\tau)\rangle_{\text{av}} \\ &\quad = \int_0^\infty \frac{d\eta\, 8G\rho_g(\eta)|B(\eta)|^2}{c^2\eta^2}\gamma(\mathbf{x}_1,\mathbf{x}_2,\eta,\tau) ,\end{aligned} \tag{4.5}$$

$$\begin{aligned}&\gamma(\mathbf{x}_1\mathbf{x}_2,\eta,\tau) \\ &\quad = \int_0^{2\pi} d\phi \int_0^\pi \sin\theta\, d\theta[(F_{1+}F_{2+}+F_{1\times}F_{2\times})] \\ &\qquad \times\cos\{[\mathbf{k}\cdot(\mathbf{x}_1-\mathbf{x}_2)+\eta\tau]\} .\end{aligned} \tag{4.6}$$

The preceding equation is the principal result of this paper. All the angular dependent terms are within γ, as it contains all the information about the relative separation and orientation of the two antennas. The value of $|\gamma|$ will range from an ideal value of $(8\pi/5)$ to zero.

C. Noise

The correlation measurement is limited by the noise in each interferometer due to a host of different sources. Most of the noise sources are expected to be uncorrelated between the interferometers (a discussion of correlated noise sources between different sites and the influence of correlated noise in interferometers operated at a single site is reserved for Sec. VI). Estimates of the noise in the interferometer are continuously being modified with improvements in the technology and more thorough understanding of the intrinsic noise sources themselves. At the time the calculations leading to this paper were made (1991) the estimates given in the proposal for the LIGO [23] based on Refs. [1,21,22] were used. In general (and this is not expected to change significantly with technological development), the noise in the interferometers is expected to be dominated by the following: ground motion transmitted through vibration isolation stages at low frequencies, thermal noise in the pendulum suspensions at middle frequencies, and photon shot noise at high frequencies. Figure 4 shows a representative noise spectrum for initial interferometers being planned for the LIGO. The interferometer is assumed to be a recycled Fabry-Perot with 5 W of laser light of wavelength 0.5145×10^{-4} cm.

In terms of the transfer function component $B(\eta)$, the shot noise limit is

$$h(f) = \frac{1}{4|B(\eta)|}\left[\frac{\hbar}{P}\omega\right]^{1/2} , \tag{4.7}$$

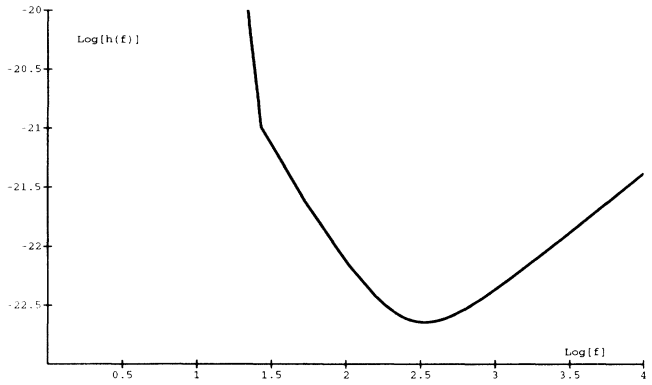

FIG. 4. Logarithm of the interferometer noise $h(f)$ vs logarithm of frequency.

where P is the laser-light power. The electric field of the laser light that exits the interferometer is proportional to the phase difference of the light beams of each arm. If the output of antenna one is given by

$$x_1(t)=z_1(t)+n_1(t) , \tag{4.8}$$

where z_1 is defined above in terms of the gravity wave and the antennas' transfer function, then the spectral density of the photon shot noise would be given by $N_1(f)=\hbar\omega/4P$, where

$$\lim_{T\to\infty}\frac{1}{T}\int_0^T n_1^2(t)dt=\int_0^\infty N_1(f)df . \tag{4.9}$$

D. Influence of noise on correlation

The presence of noise in each interferometer will affect the measured correlation. The larger the noise, the greater the uncertainty in the result. The two output signals will be expressed as

$$x_1(t)=z_1(t)+n_1(t) , \quad x_2(t)=z_2(t)+n_2(t) . \tag{4.10}$$

The noise terms n_1 and n_2 and the gravity-wave background are assumed to be stochastic and stationary with a Gaussian distribution of zero mean. The signal-to-noise ratio after a length of time T will be expressed as [4]

$$\frac{S}{N}=\frac{\langle z_1z_2\rangle_{\rm av}}{\left[(1/2T)\int_0^\infty N_1(f)N_2(f)df\right]^{1/2}} . \tag{4.11}$$

The denominator can be thought of as the variance of the correlation. The 95% confidence interval of the correlation is [24]

$$\langle z_1z_2\rangle_{\rm av}\le 1.645\left[\frac{1}{2T}\int_0^\infty N_1(f)N_2(f)df\right]^{1/2} . \tag{4.12}$$

The statistics of the correlation are explained in Sec. V.

E. Filtered data

The signal-to-noise ratio in the correlation can be improved by passing the interferometer outputs through filters. Call the filter d; it is a physically realizable filter [$d(\tau)=0$ for $\tau<0$] with its Fourier transform $D(f)$. For the case where the two interferometers have identical noise spectra and transfer functions, the filters $D(f)$ will be the same and the correlation signal is

$$\langle z_1(t)z_1(t+\tau)\rangle_{\rm av}=\int_0^\infty \frac{d\eta\, 8G\rho_g(\eta)|B(\eta)|^2|D(\eta)|^2}{c^2\eta^2}\gamma(\mathbf{x}_1,\mathbf{x}_2,\eta,\tau) , \tag{4.13}$$

while the variance of this will be

$$\sigma^2=\left[\frac{1}{2T}\int_0^\infty N_1(f)N_2(f)|D(f)|^4df\right]^{1/2} . \tag{4.14}$$

The signal-to-noise ratio can be maximized with the choice of the proper filter [25]. When one assumes that the signal is much smaller than the noise, the ideal filter will be

$$|D(f)|^2=k\frac{\rho_g(f)|B(f)|^2\gamma(\mathbf{x}_1,\mathbf{x}_2,f)}{N_1(f)N_2(f)f^2} , \tag{4.15}$$

where k is a constant. In this case the power signal-to-noise ratio after a time T will be

$$\frac{S}{N}=\frac{2G}{\pi^2c^2}\left[2T\int^\infty\left[\frac{\rho_g(f)|B(f)|^2\gamma(\mathbf{x}_1,\mathbf{x}_2,f)}{f^2}\right]^2\frac{df}{N_1(f)N_2(f)}\right]^{1/2} . \tag{4.16}$$

The limits on the energy-density background of the gravity waves can be derived from this equation. For some small frequency band spanning Δf around a frequency f, the 95% confidence limit on the gravity-wave energy density would be

$$\Omega_{\rm gw}(f)=\frac{\pi c^2f^3}{\rho_cG|\gamma(\mathbf{x}_1,\mathbf{x}_2,f)|}\left[\frac{2}{\Delta fT}\right]^{1/2}(1.645)h_n^2(f) , \tag{4.17}$$

where $h_n(f)$ is the noise spectral density of the interferometer. The limiting rms value of the strain detectable against the interferometer noise would be

$$h_{\rm rms}=\sqrt{5}\left[\frac{2\Delta f}{T}\right]^{1/4}\left[\frac{8\pi/5}{|\gamma(\mathbf{x}_1,\mathbf{x}_2,f)|}\right]^{1/2}h_n(f)\sqrt{1.645} . \tag{4.18}$$

F. Orientation and location of the antennas

The limit that one can place on the SGWB is affected by the fact that the antennas may be at different locations

and have orientations that are not mutually parallel. This effect enters the correlation through the term $\gamma(\mathbf{x}_1,\mathbf{x}_2,\eta)$, which is a function of the locations and orientations of the two detectors. For the ideal case where the two detectors are aligned and at the same location, one has $\gamma=8\pi/5$. $\gamma(\mathbf{x}_1,\mathbf{x}_2,\eta)$ may take negative values depending on the orientation of the detectors. A rotation of one of the detectors by 90° will switch the sign of γ, but leave its amplitude the same. The first interferometer pair to be considered is an example where one has two detectors separated by a continental distance. The angles used are $b_1=45.3°$ and $g_1=27°$ for detector 1, $b_2=55.1°$ and $g_2=59.9°$ for detector 2, with $a_1-a_2=50°$. This gives 40° for the angle of arc around the Earth separating the two antennas. A plot of γ vs f for this geometry is given in Fig. 5. The function γ cannot be solved in closed form for this geometry and so a numerical integration was performed. Some examples of γ are given by Michelson [26] for simple aligned but displaced detectors. The analysis presented here extends to detectors placed on a curved Earth.

Note that there are certain frequencies for which γ is zero. It is impossible to perform a correlation measurement at these frequencies. The zeros fall at about 37 and 75 Hz and repeat about every 70.6 Hz after these values. The frequency 70.6 Hz corresponds to the distance between the two sites, 4.25×10^8 cm, divided by c. At low frequencies γ takes on its maximum amplitude of 3.92. The next extrema occurs at 52 Hz with a value of 0.89, followed by a value of -0.41 at 90 Hz. Extrema then occur near $52+70.6n$ and $90+70.6n$ Hz, where n is some integer. It has been stated [23] that the rms value of the strain h that two detectors can detect is proportional to $\sqrt{1+fD/c}$, which would imply that γ should be proportional to $(1+fD/c)^{-1}$, where d is the distance between the antennas. This is not a fast enough decrease. It turns out that for the detector-1–detector-2 geometry the amplitudes at the extrema fall more like $(1+fD/c)^{-2}$, implying that the rms value of the detectable strain should go as $(1+fD/c)$. This can be seen in Fig. 6. Envelope 1 is made up of the curves $\pm3.92/(1+fD/c)$, while envelope 2 is made up of the curves $\pm3.92/(1+fD/c)^2$. Both curves have the low-frequency value of 3.92, and

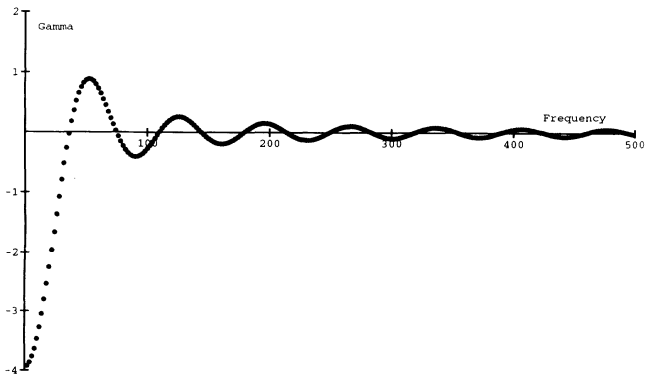

FIG. 5. Plot of γ vs frequency (in Hz) for the geometry of $b_1=45.3°$ and $g_1=27°$ for detector 1, $b_2=55.1°$ and $g_2=59.9°$ for detector 2, with $a_1-a_2=50°$.

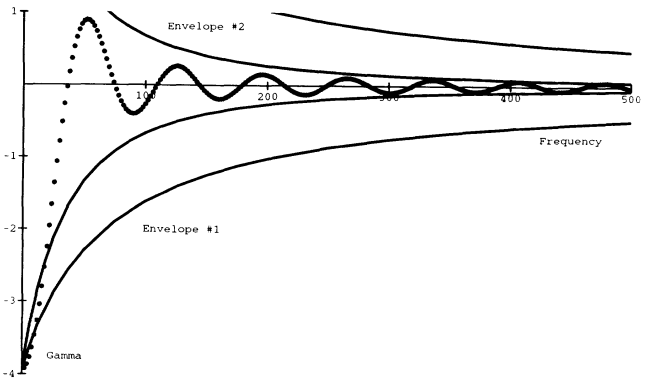

FIG. 6. Plot of γ vs frequency (in Hz) for the detector-1–detector 2 geometry along with envelopes 1 and 2.

the distance used is 4.25×10^8 cm.

The location of the zeros for the correlation can be changed by changing the orientations of both interferometers. If one of the detectors is aligned such that one of its arms points along the great circle connecting the two detectors, the location of the zeros cannot be changed by rotating the second detector. This is illustrated in Fig. 7 for the detector-1–detector-2 geometry. The orientation of one of the detectors is allowed to rotate from the optimum orientation whereby both detectors have an arm along the great circle connecting them. The only effect of the rotation is to seriously decrease the amplitude of γ. Next consider the case where an interferometer's orientation is fixed at some position other than that where an arm lies along the great circle. As an illustration, consider detector 1 with a fixed value of $g=27°$. The orientation of detector 2 is allowed to change from the optimum value of $g=59.9°$. Figure 8 shows the result. The low-frequency zeros move slightly, while at higher frequencies the zeros converge back together. The amplitude of γ is seriously reduced by doing this. The proposed kilometer-length interferometers will not be rotatable antennas. Once built, their orientation will be fixed. It is not known what the spectrum of the SGWB will look like, but one may reasonably assume that it will be fairly

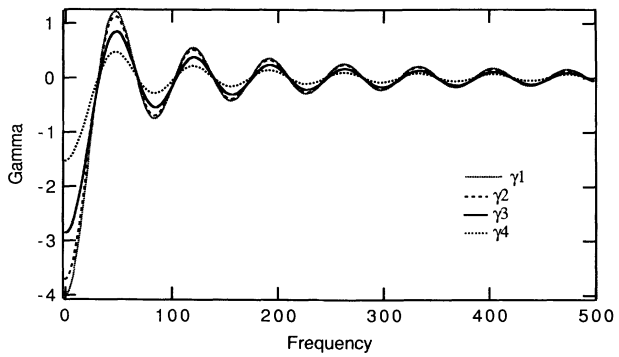

FIG. 7. Plot of γ vs frequency (in Hz) for the detector-1–detector-2 geometry. Detector 1 interferometer has one arm along the great circle connecting the two sites. The other interferometer has an arm along the great circle for $\gamma1$, an arm 11.25° off the great circle for $\gamma2$, 22.5° for $\gamma3$, and 33.75° for $\gamma4$. Note that the zeros do not move.

colorless over the range of frequencies in which these detectors will operate. In order to maximize the probability of detecting the SGWB, one should orient the interferometers so that the envelope of γ is maximized, namely, find the extrema of Eq. (3.7). One can change the zeros, but only at the expense of seriously reducing the γ's amplitude. At a given frequency the optimum orientation may be different than the one which gives an extrema of Eq. (3.7). However, the most important criteria should be to detect the SGWB at those frequencies which maximize the probability of detection, not at some other randomly chosen frequency. One should conduct a search for the SGWB at those frequencies where γ has a local extrema.

It should also be pointed out that introducing a delay τ in the correlation will not change the location of the zeros. It can be shown that

$$\gamma(\mathbf{x}_1,\mathbf{x}_2,\eta,\tau)=\int_0^{2\pi}d\phi\int_0^{\pi}\sin\theta\,d\theta(F_{1+}F_{2+}+F_{1\times}F_{2\times})\cos\{[\mathbf{k}\cdot(\mathbf{x}_1-\mathbf{x}_2)+\eta\tau]\}$$
$$=\cos\eta\tau\int_0^{2\pi}d\phi\int_0^{\pi}\sin\theta\,d\theta(F_{1+}F_{2+}+F_{1\times}F_{2\times})\cos\{[\mathbf{k}\cdot(\mathbf{x}_1-\mathbf{x}_2)]\}\ . \tag{4.19}$$

Once the orientation of the two detectors is fixed, the zeros are also fixed.

In the case when the two detectors are located on different sides of the Earth, it is possible to solve for the γ term exactly. For detectors that are aligned and separated by $2R$, where R is the Earth's radius, one has

$$\gamma=\cos[4\pi fR/c]\left\{\frac{c^2}{2\pi f^2R^2}-\frac{3c^4}{64\pi^3f^4R^4}\right\}$$
$$+\sin[4\pi fR/c]\left\{\frac{c}{fR}-\frac{3c^3}{16\pi^2f^3R^3}+\frac{3c^5}{256\pi^4f^5R^5}\right\}. \tag{4.20}$$

For frequencies of hundreds of Hz, the envelope appears to go as $(1+fD/c)^{-1.5}$. From the above expression one can see that the envelope will eventually go as $(1+fD/c)^{-1}$ at high frequencies. The character of γ is much more complicated than what was previously assumed.

There are other groups around the world that are planning to build interferometric gravity-wave antennas. The antenna that will probably be closest in distance to the planned detectors in the United States will be constructed in Europe. For the purpose of an example, γ is calculated for a correlation between sample antennas separated by North American (detectors 1 and 2) to European (detector E) distance scales. The orientation of detector E is chosen so that it is optimally aligned with detector 1. The angles for detector E are $b_3=42°$ $g_3=55.9°$ $a_3-a_1=79.3°$ and $a_3-a_2=129.3°$. This gives 52.3° for the angle of arc around the Earth separating detectors 1 and E, and 85.5° for detectors 2 and E. The γ for the two correlations are illustrated in Figs. 9 and 10. The low-frequency value for the detector-1–detector-E γ is -3.43, while for detector-2–detector-E it is -2.14.

Note that the extrema for the three γ's calculated in this section are located at different places. This will help in extracting a SGWB limit at certain frequencies. When the extrema for the three γ's coincide at some frequency, a three-way correlation can be utilized, and the limit on $\Omega_{gw}(f)$ at that frequency will be reduced by $\sqrt{3}$. This would be the case at $f=92$ and 198 Hz in the current example. However, an extrema for one pair may result in a null value for the others. This is the case for the extrema at 172 Hz for the detector-1–detector-E correlation. The other two γ's are near zero there. There are cases where two extrema occur near each other, as happens at $f=126$ and 146 Hz, and one gains by a factor of $\sqrt{2}$ in the limit of $\Omega_{gw}(f)$. In summary, adding a third detector increases the accessible frequency regime, more extrema are pro-

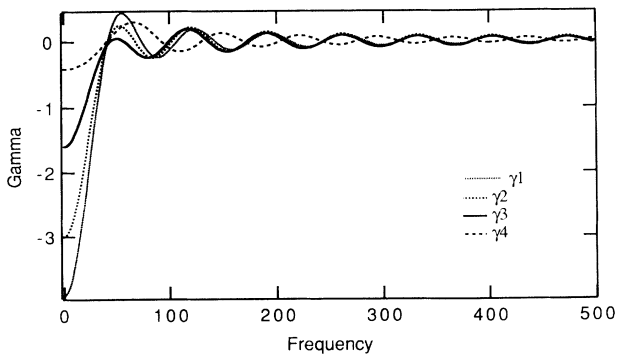

FIG. 8. Plot of γ vs frequency (in Hz) for the detector-1–detector-2 geometry. Detector 1 interferometer has one arm at $g_1=27°$. The other interferometer has one arm $g_2=59.9°$ for $\gamma1$, $g_2=76.9°$ for $\gamma2$, $g_2=89.9°$ for $\gamma3$, and $g_2=104.9°$ for $\gamma4$. Note that the zeros move at low frequencies, but converge together at higher frequencies.

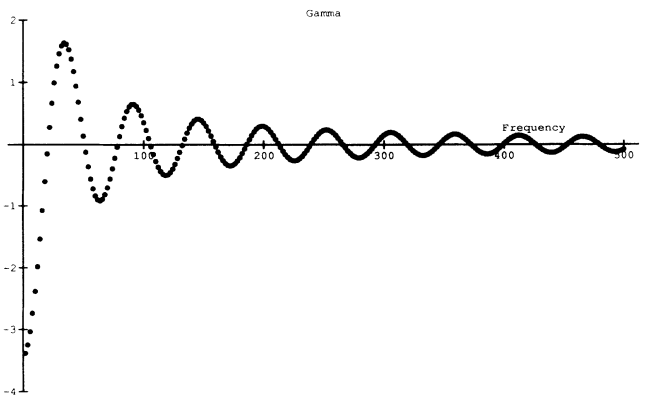

FIG. 9. Plot of γ vs frequency (in Hz) for the geometry of $b_1=45.3°$ and $g_1=27°$ for detector 1, $b_2=42°$ and $g_2=55.9°$ for detector E, with $a_3-a_1=79.3°$.

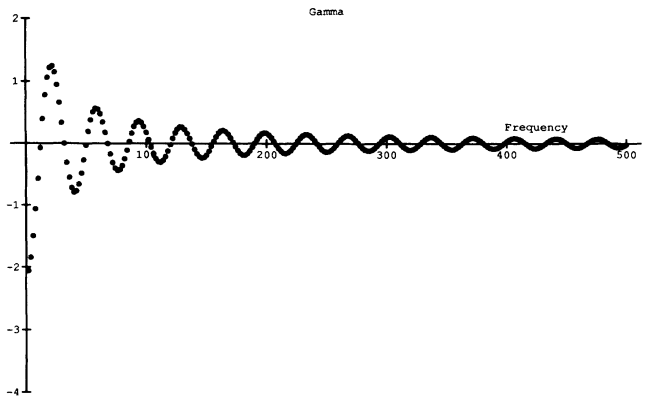

FIG. 10. Plot of γ vs frequency (in Hz) for the geometry of $b_2=45.3°$ and $g_2=59.9°$ for detector 2, $b_2=42°$ and $g_2=55.9°$ for detector E, with $a_3-a_2=129.3°$.

vided, and the null areas begin to get covered. In some cases the extrema overlap and a nontrivial increase in sensitivity is achieved.

G. Sensitivity limits

The correlation sensitivity for some sample interferometers using reasonable parameters is presented in this section. The initial long-baseline interferometers may be shot-noise limited above about 200 Hz with 5 W of 0.5145-nm laser light in a recycled Fabry-Pérot system. Figure 4 shows the interferometer noise predicted for the sample system investigated here. The planned long-baseline interferometer systems hope to employ more advanced techniques as the technology is developed. It is hoped that a recycled Fabry-Pérot with 60 W of 0.5145-nm light will be shot-noise limited above 100 Hz. In addition, a narrow-band dual recycling system is intended to be used with 60 W of light [23,27].

The 95% confidence limit achieved by the correlation between a full- and half-length system at a particular site is illustrated in Fig. 11. This plot shows the sensitivity of the three interferometer systems, the initial recycled Fabry-Pérot (No. 1), the advanced recycled Fabry-Pérot (No. 2), and the envelope for the advanced dual-recycling Fabry-Pérot (No. 3). The rms value of the strain sensitivity is given by

$$h_{\rm rms}=\sqrt{5}\left[\frac{2\Delta f}{T}\right]^{1/4} h_n(f)\sqrt{2\times 1.645}\ , \qquad (4.21)$$

where it is assumed that the bandwidth Δf of the measurement is equal to the frequency f and it has been assumed that $T=10^7$. Also shown is the sensitivity in terms of the energy density of the SGWB, $\Omega_{\rm gw}(f)$.

Figure 12 illustrates the sensitivity for the three interferometer designs, but where the full-length antennas are located in the detector-1–detector-2 geometries defined above. The rms value of the strain sensitivity is given by Eq. (4.18), where γ for the detector geometry is exhibited in Sec. IV F and Fig. 5.

There is another point that should be raised about the limit one places on $h_{\rm rms}$ or $\Omega_{\rm gw}(f)$. The standard prac-

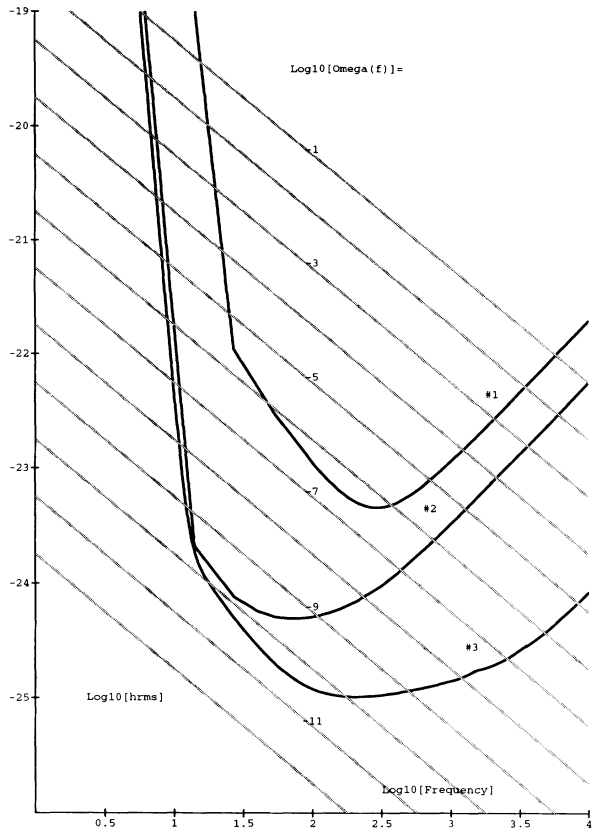

FIG. 11. Plot of sensitivity to $h_{\rm rms}$ and $\Omega_{\rm gw}(f)$ (diagonal gray lines) vs frequency for the initial recycled Fabry-Pérot (No. 1), the advanced recycled Fabry-Pérot (No. 2), and the envelope for the advanced dual-recycling Fabry-Pérot (No. 3). This assumes a 4- and a 2-km interferometer at the same site.

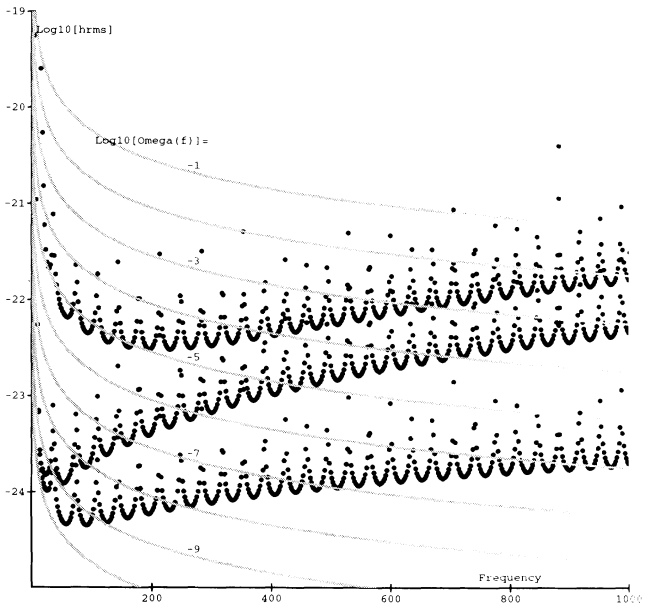

FIG. 12. Plot of sensitivity to $h_{\rm rms}$ and $\Omega_{\rm gw}(f)$ (gray lines) vs frequency for the initial recycled Fabry-Pérot (No. 1), the advanced recycled Fabry-Pérot (No. 2), and the envelope for the advanced dual-recycling Fabry-Pérot (No. 3) for the detector-1–detector-2 geometry.

tice is to read the values from formulas (4.17) and (4.18) and assume that the bandwidth of the measurement Δf is about the same as the frequency at which the measurement is concentrating. This is an approximation that works well for broadband detection, but is incorrect for a narrow-band measurement, such as dual recycling. When optimum filter techniques are applied to the outputs of each antenna, then the 95% confidence limit is given by formula (4.16), with $S/N=1.645$. For dual recycling the effective bandwidth is much smaller than the frequency where the measurement is taking place. One cannot approximate the integral by assuming a $\Delta f \approx f$. Figure 13 shows the result of this. The sensitivity of the advanced recycling Fabry-Pérot (No. 2) and the advanced dual-recycling Fabry-Pérot (No. 3) systems according to the approximation $\Delta f = f$ are plotted against $\Omega_{\rm gw}(f)$. The dots show the result when the optimum filter output is properly integrated over frequency. The actual dual-recycling limit is not quite as good as what one would normally expect.

The LIGO system plans to expand the number of interferometers at each site as a later development [23]. The plan is to have three full-length and three half-length interferometers at one location and three full-length interferometers at the other site. This will result in 36 correlations. Section V explains the statistics of a multiple correlation with the use of the multivariate normal distribution. Out of the 36 correlations, 18 will be from two detectors at a similar site, called "near correlations," while the other 18 will be from having the detectors at different sites, called "far correlations."

For the near correlations, six will be from full-length–full-length pairs, nine from full-length–half-length pairs, and three from half-length–half-length pairs. This will result in a decrease in the limit for $\Omega_{\rm gw}(f)$ of 5.8 over the single full-length–half-length correlation. As an example, consider the advanced dual-recycling system with the bandwidth properly accounted for. At 100 Hz the single full-length–half-length correlation of 10^7 s limits the SGWB energy density to

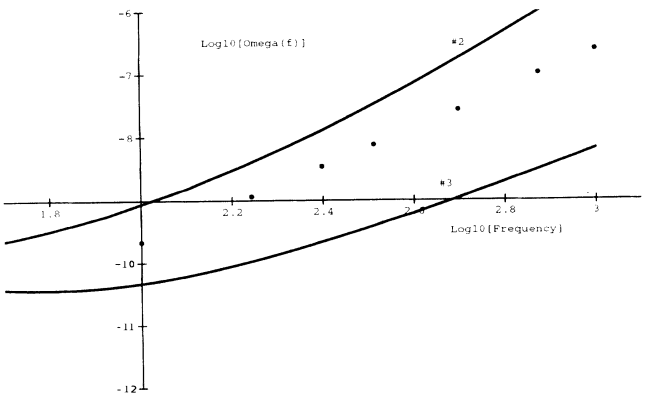

FIG. 13. Solid lines show the sensitivity to $\Omega_{\rm gw}(f)$ for the advanced recycling Fabry-Pérot (No. 2) and the advanced dual-recycling Fabry-Pérot (No. 3) according to the approximate solution where $\Delta f = f$. The dots show the result when the optimum filter output is properly integrated over frequency.

$\Omega_{\rm gw}(f)=2\times10^{-10}$, while for all 18 near correlations the limit would be $\Omega_{\rm gw}(f)=4\times10^{-11}$.

For the far correlation there will nine full-length–full-length pairs and nine full-length–half-length pairs. This will result in a decrease in the limit for $\Omega_{\rm gw}(f)$ of 3.67 over the single full-length–full-length correlation. As an example, consider an advanced dual-recycling system. At 126 Hz, where there is an extrema in γ, the single full-length–full-length correlation of 10^7 s limits the SGWB energy density to $\Omega_{\rm gw}(f)=5.5\times10^{-9}$, while for all 18 near correlations the limit would be $\Omega_{\rm gw}(f)=1.5\times10^{-9}$.

V. STATISTICS AND MULTIPLE DETECTORS

A. Two-detector statistics

Consider two time series. Each series is composed of the signal s and its noise n. The ith component of the time series for detectors Nos. 1 and 2 is given by

$$x_{1i}=s_i+n_{1i}\ ,\quad x_{2i}=s_i+n_{2i}\ . \tag{5.1}$$

It is assumed that the terms s, n_1, and n_2 are all independent stationary Gaussian random processes with zero mean. A correlation will be calculated to determine the variance of s, σ_s^2. The variance σ_s^2 is assumed to be much smaller than the variance for either noise term σ_{n1}^2 or σ_{n2}^2. The correlation will be determined from a string of N data points from the bivariate normal distribution via

$$r=\frac{\sum_{i=1}^{N} x_{1i}x_{2i}}{\left[\left(\sum_{i=1}^{N} x_{1i}^2\right)\left(\sum_{i=1}^{N} x_{2i}^2\right)\right]^{1/2}}\cong\frac{\sigma_s^2}{\sigma_{n1}\sigma_{n2}}\ . \tag{5.2}$$

Before it is possible to make a definite detection of σ_s^2, one will want to place a limit on its size. To do this in a statistically proper way, one should use the Neyman-Pearson lemma [24].

The Neyman-Pearson approach compares two hypotheses: the null hypothesis H_0 and the alternative hypothesis H_1. From the data set one would like to determine which hypothesis can be supported. If the true state is either H_0 or H_1, then one can make two types of errors. A type-I error is when H_0 is actually the correct state, but the data lead one to declare that H_1 is the true state. A type-II error is when H_1 is the correct state but one declares H_0 to be true. The probability for a type-I error is α, while the probability for a type-II error is β. The probability α is called the "level of significance of the test." The term $1-\beta$ is called the "power of the test."

The Neyman-Pearson test can be used to put a limit on the size of the correlation between two detector signals. The data will be used to test the null hypothesis $H_0{:}r=0$ against the alternative hypothesis $H_1{:}r\neq0$. Under the assumption that $r=0$, the variable

$$t=r\left[\frac{N-2}{1-r^2}\right]^{1/2} \tag{5.3}$$

has a Student-Fisher t distribution with $N-2$ degrees of freedom. When one demands a probability of 0.05 for a

type-I error, $N \gg 1$, and the sign of the correlation is known (positive, for example), then the limit on r and σ_s will be

$$r \leq \frac{1.645}{\sqrt{N}} , \quad \sigma_s^2 \leq \frac{1.645\sigma_{n1}\sigma_{n2}}{\sqrt{N}} . \tag{5.4}$$

The correlation that is being tested for in this example is either zero or positive. The probability of rejecting the hypothesis $H_1: r \neq r_0$ and $r > 0$ when it is actually true and one has chosen $\alpha = 0.05$ is β. The power for the hypothesis $r > 0$ is

$$1-\beta = \frac{1}{2}\left[1+\text{erf}\left[\frac{1}{\sqrt{2}}\{1.645 - r\sqrt{N}\}\right]\right] . \tag{5.5}$$

If it suspected that there is some positive correlation r_0, one can also apply the Neyman-Pearson lemma. The null hypothesis is $H_0: r = r_0$, while the alternative hypothesis is $H_1: r \neq r_0$, where the alternative hypothesis can be expanded to two alternative phyotheses: namely, $H_1': r > r_0$ or $H_1'' r < r_0$ [24]. When N data points from two detectors are correlated, the result will be one number r. The first task to take is to see if this number is consistent with zero. For a level of significance of 0.05, any value of r such that $r < 1.645/\sqrt{N}$ is consistent with the actual correlation r_0 being zero. However, for the same level of significance, there is a spread of values for r_0 that can be acceptable. For a measured value r, there will be a probability of 0.95 that r_0 is in the interval

$$\frac{-1.96}{\sqrt{N-3}} + r < r_0 < r + \frac{1.96}{\sqrt{N-3}} . \tag{5.6}$$

The ideal scenarios presented above will differ from the real case when one has data from two antennas. The correlated output of two detectors in some bandwidth Δf will be

$$\frac{1}{N}\sum_{i=1}^{N} x_{1i}x_{2i} = \frac{8G}{c^2}\int^{\Delta f} df \frac{\rho_g(f)}{(2\pi f)^2}[B_1 B_2^* + B_1^* B_2]\gamma(f) . \tag{5.7}$$

The equivalent 95% confidence limit after a total integration time is T will be

$$\frac{8G}{c^2}\int^{\Delta f} df \frac{\rho_g(f)}{(2\pi f)^2}[B_1 B_2^* + B_1^* B_2]\gamma(f) \leq 1.645\left[\frac{1}{2T}\int^{\Delta f} N_1(f)N_2(f)df\right]^{1/2} . \tag{5.8}$$

B. Multiple detectors

Consider M detectors, with N data points from each detector, and each output is the sum of the signal and the detector's intrinsic noise. The ith data point of the jth detector is $x_{ji} = s_i + n_{ji}$. There will be $M(M-2)/2$ correlations. The correlation between the ith and jth detector's data is given by r_{ij}. Assume that the variance of the independent Gaussian noise in each detector is the same. The null hypothesis for the Neyman-Pearson test will be $H_0: r_{ij} = 0$ for all i and j, while the alternative hypothesis is $H_1: r_{ij} \neq 0$ for all i and j. An approximate test statistic can be given by a χ^2 with one degree of freedom [24]:

$$\chi^2 = \left[N - 1 - \frac{2M+5}{6}\right]\sum_{i<j}\sum r_{ij}^2 . \tag{5.9}$$

In general, the strength of the correlation will not be the same for all pairs of detectors. In the multiple gravity-wave antenna problem, the correlations will be different for different detector pairs, but the ratios of the correlations will be calculable. It is the relative orientation of the detectors, their displacement from one another, their individual transfer functions, and their intrinsic noise that will change the correlation strength. These effects can all be calculated or measured. However, all the detectors are responding to the same SGWB. It is the magnitude of this background which is the uncertainty.

The correlation between the signal from detectors i and j will be given by

$$r_{ij} = \frac{a_{i,j}\sigma_s^2}{\sigma_{ni}\sigma_{nj}} = \alpha_{i,j}\sigma_s^2 . \tag{5.10}$$

The term a_{ij} takes into account the difference in response of each interferometer pair, while $\alpha_{ij} = a_{ij}/(\sigma_{n1}\sigma_{n1})$. We can use the same null hypothesis of $r = 0$ to be tested against the alternative hypothesis of $r \neq 0$. Because the signs of all the a_{ij} are known, one can attribute the 2α value of this variate for an α-level test. For a type-I error level of 0.05, and where $N \gg 1$, a limit on σ_s^2 will be given by

$$\sigma_s^2 \leq \sigma_n^2(1.645)\left[\frac{1}{N(\alpha_{1,2}^2 + \cdots + \alpha_{M-1,M}^2)}\right]^{1/2} . \tag{5.11}$$

There are $M(M-1)/2$ correlation terms in the denominator inside the radical. The power of this test for a $\sigma_s^2 > 0$ hypothesis is

$$1-\beta = \frac{1}{2}\left[1-\text{erf}\left[\frac{1}{\sqrt{2}}\{1.645 - \sigma_s^2[N(\alpha_{1,2}^2 + \cdots + \alpha_{M-1,M}^2)]^{1/2}\}\right]\right] . \tag{5.12}$$

In the case of actual gravity-wave antenna data being correlated, the σ_s^2 will correspond to the energy density of the SGWB. For some bandwidth Δf around the frequency f, the energy density of the SGWB would be $\sigma_s^2 = \rho_g(f)\Delta f$, while the $\alpha_{i,j}$ terms are given by

$$\alpha_{i,j} = \frac{8G[B_i B_j^* + B_i^* B_j]\gamma_{ij}(f)}{c^2(2\pi f)^2\sqrt{N_1(f)N_2(f)}(\Delta f)} , \tag{5.13}$$

where N can be expressed as $N = 2T\Delta f$.

As an example, consider two identical detectors at the

same location. This will make $\gamma=8\pi/5$. The antennas will be the broadband recycling Fabry-Pérot interferometers with 60 W of laser-light power and an arm length of 4 km. Say the total integration time is 10^7 s and that $f=\Delta f=150$ Hz. Assuming that the energy density of the gravity waves is very small and that a level of significance of $\alpha=0.05$ for the hypothesis $\sigma_s^2=0$ is desired, this system will be able to limit the ratio of gravity-wave energy density per unit logarithmic interval of frequency to critical energy density to $\Omega_{\rm gw}(f)\leq 1.8\times 10^{-9}$. On the other hand, say a value of $\Omega_{\rm gw}(f)=10^{-7}$ is derived from the measured correlation. This is about the value that one would expect from a background of cosmic strings that were responsible for galaxy formation. The power for the hypothesis that $\sigma_s^2>0$ and $\Omega_{\rm gw}(f)>0$ would be effectively 1. There would be no doubt about accepting the alternative hypothesis. The range of possible values for the true energy-density background that would be allowed by this measurement at a level of significance of 0.05 would be $9.6\times 10^{-8}<\Omega_{\rm gw}(f)<1.04\times 10^{-7}$.

The LIGO system [23] will consist of two 4-km-arm-length interferometers at different locations, and a half-length interferometer at one of the sites. This three-detector system will be considerably different than the simple model above. While one of the full-length interferometers will be at the same location and at the same orientation as the half-length antenna, the second full-length detector will be located on the other side of the country. Not only will the orientation of the detectors be different, but the correlation function will have a frequency dependence to it.

As an example, consider the case where a single full-length detector is the above-defined detector 1, while a full-length (detector 2) and half-length (detector 3) system is located at the above-defined detector-2 site. The orientation of the detectors and the frequency dependence of the correlation were chosen according to the method discussed above. At 126 Hz there is a local maximum in the frequency dependence of the correlation function. This is where this example will be carried out. Assume that the noise spectrum will be the same for all three detectors.

The three expected correlations, up to a common constant, are $r_{12}=0.104r_0$, $r_{13}=5.2\times 10^{-2}r_0$, and $r_{23}=r_0$. The calculation of these values considered the lengths of the interferometers, relative orientations, and distance separations. The limit of the size of r_0 via the three-channel multivariate normal method to a level of significance of 0.05 would be $r_0\leq 1.634/\sqrt{N}$, while if one used only the one correlation from the full- and half-length systems at the same location the limit would be $r_0\leq 1.645/\sqrt{N}$. One hardly gains anything over the two detectors at the same location scenario. The ideal case of a correlation from two interferometers at the same location is much better than the correlation from two antennas separated by a continental displacement. Of course, correlated noise at this common location has been ignored for this example. Note that since the correlation r_{12} is 10 times smaller than the correlation r_{23} it will take 100 times longer to place the same limit on the energy density with r_{12} than by using r_{23}. The limit goes as

$$\frac{1}{\sqrt{N}}=\frac{1}{\sqrt{2T\Delta f}}\ . \tag{5.14}$$

C. Correlated noise at a similar site

The full- and half-length combination at one site appears to be a very convenient arrangement. However, there will almost certainly be some common correlated noise. This will be from such things as seismic noise, electric power fluctuations, or residual gas pressure since the two interferometers will be in the same vacuum system. This will hinder the task of extracting the signal. Whatever the cause of the correlated noise, it will place a limit on the measurement.

Consider the two data streams

$$\begin{aligned} x_{1i}&=s_i+n_{1i}\ , \\ x_{2i}&=\tfrac{1}{2}s_i+n_{2i}\ . \end{aligned} \tag{5.15}$$

Next, call

$$\langle n_1 n_2\rangle_{\rm av}=\frac{1}{N}\sum_{i=1}^{N}x_{1i}x_{2i}=\rho\sigma_{n1}\sigma_{n2}\ . \tag{5.16}$$

The correlation between channels 1 and 2 will be

$$\begin{aligned} r_{12}&=\frac{\frac{1}{2}\sigma_s^2+\rho\sigma_{n1}\sigma_{n2}}{[(\sigma_s^2+\sigma_{n1}^2)(\frac{1}{4}\sigma_s^2+\sigma_{n2}^2)]^{1/2}} \\ &\cong\frac{\frac{1}{2}\sigma_s^2+\rho\sigma_{n1}\sigma_{n2}}{\sigma_{n1}\sigma_{n2}}\ . \end{aligned} \tag{5.17}$$

It was assumed that the noise variance is much bigger than the signal's variance. So the correlated noise will contribute as much to the correlation as the signal when $\rho=\sigma_s^2/(2\sigma_{n1}\sigma_{n1})$. For a numerical example, say there is a background energy density of gravity waves that has $\Omega_{\rm gw}(f)=10^{-7}$, about that which would be produced from cosmic strings. The detectors will be the broadband recycling Fabry-Pérot interferometers with 60 W of laser-light power and arm lengths of 4 and 2 km. At 150 Hz the signal variance to noise variance would be 1.66×10^{-3}, and so a correlation between the two noise terms of $\rho=8.3\times 10^{-4}$ would mask the signal.

VI. COMMON NOISE IN DIFFERENT INTERFEROMETERS

The extraction of the SGWB signature from the correlated output of two interferometers can be limited by the presence of a noise source common to each detector. Common noise will contribute to the correlation. This problem will be more severe for the case where two interferometers are at the same site and in the same vacuum system. This is also the case where one has the most potential sensitivity, and so it is important to see how bad the limitations will be. The existence of a problematic coherent noise source for two detectors separated by thousands of kilometers seems unlikely, but is not completely excluded. The likely problematic noise sources are considered.

A. Seismic noise

Seismic noise will contribute to the noise spectrum of the interferometric antenna. The ground motion will cause the mirror masses to move as the vibration propagates through the isolation and suspension system. This motion of the mirrors will mimic the effect of a gravity wave. Two interferometers at the same site will each respond to the same seismic wave. This will certainly be a problem at some level. The influence of seismic waves on a correlation decreases as the interferometers are displaced from one another.

Consider a full- and a half-length interferometer a certain site. Also, consider a stochastic background of surface seismic waves, which propagate at velocity v_s ($1 < v_s < 10$ km/s). Most seismic waves are surface waves [28]. This stochastic background of surface seismic waves is assumed to follow the same stationary and ergodic assumptions that were applied to the gravity waves. For simplicity, both the longitudinal and transverse components of the seismic displacement will be lumped together. The spectral density for the seismic noise is expected to be on the order of

$$S_s(f)=10^{-10}\ \mathrm{cm^2/Hz}\left[\frac{1\ \mathrm{Hz}}{f}\right]^4, \tag{6.1}$$

for frequencies above 10 Hz.

The vibration isolation system will attempt to isolate the masses from this ground noise. Consider a five-layer stack of elastomer springs and masses,with a pendular suspension that holds the mirror. The system will have a transfer function of

$$T(f)=\left[\frac{1\ \mathrm{Hz}}{f}\right]^2\left[\frac{7\ \mathrm{Hz}}{f}\right]^{10}, \tag{6.2}$$

for horizontal isolation and for frequencies above tens of hertz [23]. The proposed transfer function for vertical isolation is

$$T(f)=\left[\frac{6\ \mathrm{Hz}}{f}\right]^2\left[\frac{15\ \mathrm{Hz}}{f}\right]^{10}, \tag{6.3}$$

for frequencies above about 10 Hz [23]. The limit on the energy density of the SGWB that can be detected by the full-length–half-length system at the same site that is also contaminated by seismic noise is given by

$$\Omega_{\mathrm{gw}}(f)=\frac{5\pi c^2 f^3}{2G\rho_c L^2}S_s(f)|T(f)|^2\left[\left\{J_0\left[\frac{2\pi fL}{v_s}\sqrt{5/4}\right]^{1/2}-J_0\left[\frac{\pi fL}{v_s}\right]-2J_0\left[\frac{2\pi fL}{v_s}\right]+2\right\}^2+\left\{J_0\left[\frac{\pi fL}{v_s}\right]+J_0\left[\frac{2\pi fL}{v_s}\sqrt{5/4}\right]\right\}^2\right]^{1/2}. \tag{6.4}$$

This limit is independent of the length of integration time and the type of interferometer used. If the isolation system operates as well as intended, seismic noise will not be a problem. The full-length–half-length system will be able to limit the SGWB energy density to a level of $\Omega_{\mathrm{gw}}(f)\sim 10^{15}$ at 100 Hz if seismic noise were the dominant noise source [19].

B. Fluctuations in the residual-gas column density inside the common vacuum system

Another noise source to consider is from the column-density fluctuations of the residual gas in the vacuum system. A column-density fluctuation will change the number of molecules in the laser-light beam, and this in turn will change the index of refraction and, thereby, the phase of the light. This effect will produce coherent noise in two interferometers only when they are both in the same vacuum system. The primary cause of these fluctuations will be from bursts of gas from the walls of the system. These bursts will have a unique signature and may be identifiable in the output data or from monitoring devices such as UV-absorption spectroscopy [23]. If the gas burst can be identified,then the data from the time of the burst can be removed. Otherwise, it will add to the value of the correlation.

The column-density fluctuation $\delta\sigma$ is the change in the number of molecules per cm^2. If there is a gas burst containing N molecules, then one has $\delta\sigma=N/A$, where A is the cross-sectional area of the beam tubes. The noise induced in an interferometer due to these fluctuations is given by $h_n(f)=2\pi\alpha\delta\sigma(f)/L$, where α is the polarizability of the molecule, $\delta\sigma(f)$ is the spectral density of the fluctuation in molecules per cm^2 per $\sqrt{\mathrm{Hz}}$, and L is the full-length interferometer's arm length. The gas bursts would be expected to consist of N_2, H_2O, or H_2 molecules.

Since the beams for each interferometer are within the same vacuum, the noise induced from a fluctuation is assumed to affect each beam by the same amount. This is a worst-case scenario. In order for the column-density fluctuations to contribute as much to the correlation of the output data as the SGWB, one must have

$$\Omega_{\mathrm{gw}}(f)=\frac{5c^2\pi^3 f^3\alpha^2\delta\sigma^2(f)}{L^2\rho_c G}. \tag{6.5}$$

For an $L=4$ km system with the N_2 value of $\alpha=1.6\times10^{-24}$ cm^3, one can limit $\Omega_{\mathrm{gw}}(f)$ to smaller than 2×10^{-9} if the column-density-fluctuation spectral density is smaller than 10^3 molecules per cm^2 per $\sqrt{\mathrm{Hz}}$.

The signature of an individual gas burst that the laser beam sees is expected to be quite unique [29]. The fluctuation will rise from zero to $\delta\sigma(0)$ in a simple t_0 given by $t_0=2w/v_{\mathrm{th}}$, where W is the $1/e$ radius of the beam and v_{th} is the thermal velocity of the gas. The decay time

for the burst is given by $T=V/F$, where F is pumping speed for the vacuum system and V is the volume. For the LIGO system the expected values are $t_0 \approx 1.2\times10^{-4}$ s and $T=100$ s [23].

The column-density-fluctuation signal $\delta\sigma(t)$ can be Fourier transformed to yield the spectral density. If there is a burst with peak magnitude $\delta\sigma(0)$ every τ seconds, then the spectral density is $\delta\sigma(f)=\delta\sigma(0)|\Sigma(f)|/\sqrt{\tau}$, where $\Sigma(f)$ is Fourier transform of the unit amplitude signal $\delta\sigma(t)$. For $f=100$ Hz, a limit of $\Omega_{\rm gw}(f)=2\times10^{-9}$ can be achieved if $\delta\sigma(0)/\tau^{1/2}<6.25\times10^{5}$. For this limit on $\Omega_{\rm gw}(f)$, one could tolerate a burst producing a column-density change of 6.25×10^{5} N_2 molecules per cm^2 every second.

C. Magnetic-field fluctuations

The next type of noise to be considered is that due to fluctuating magnetic fields. This could be the major source of correlated noise for a full-length–half-length system at one site. It may even be a problem for two detectors that are separated by thousands of kilometers. There are a number of sources of magnetic-field fluctuations in the regime around 100 Hz. Power lines will carry and propagate disturbances. Lightning will create impulsive events that can be detected thousands of miles away. The Earth and ionosphere form a resonant cavity that allows magnetic disturbances to propagate and resonate at certain frequencies. Ionospheric currents cause magnetic noise that propagates down to the Earth along field lines and can be detected simultaneously at the North and South poles and at midlatitudes.

The force on a magnetic dipole $\boldsymbol{\mu}$ by an external magnetic field $\mathbf{B}$ is $\mathbf{F}=\nabla(\boldsymbol{\mu}\cdot\mathbf{B})$. The dipole moment for a mirror mass will be caused by magnets attached to it. These magnets are to be used as magnetic pushers for the isolation system. If the magnetic pushers are not used, the major source of a dipole moment will be due to iron impurities. The amount of iron in premium-quality fused silica can be as high as 5 parts per 10^6 [30]. In order for a force to be experienced, it is necessary for there to be a spatial dependence in $\mathbf{B}$. The gradient in the magnetic field will be caused by the presence of ferromagnetic materials that are near the mass and thereby distort the background field.

If the position displacement of the mass m and dipole moment μ, is $x(f)$, in cm/$\sqrt{\rm Hz}$ and the spectral density of the force is $F(f)$ in dyn/$\sqrt{\rm Hz}$, then

$$x^2(f)=\frac{F^2(f)}{m^2(2\pi f)^4} . \tag{6.6}$$

The divergence of the magnetic-field spectral density $B_m(f)$ G/$\sqrt{\rm Hz}$ is approximated by $\nabla B_m(f)\sim B_m(f)/l$, where l is the characteristic distance to the ferromagnetic objects that will disrupt the field. The noise limit in the gravity-wave strain, $h(f)$, for the interferometer of length L with four masses is

$$h(f)\approx\frac{F(f)}{2Lm(\pi f)^2}\approx\frac{\mu B_m(f)}{2Lm(\pi f)^2 l} . \tag{6.7}$$

For a system with a full-length–half-length system at one site, the central masses will be only about 15 m from each other. These two central masses will respond to the same magnetic-field fluctuation. In this case the best limit that can be placed on the energy density of the gravity-wave background is

$$\Omega_{\rm gw}(f)=\frac{5c^2\mu^2B_m^2(f)}{16\pi^3L^2m^2l^2G\rho_c f} . \tag{6.8}$$

Some sensible values for the interferometer will be $m=10$ kg, $l=5$ m, and $L=4$ km. The dipole moment μ for the mass is defined by the characteristics of the magnets used. If one has a total of two magnets per mass, each of which has $B_0=500$ G and a volume of $V=0.1$ cm^3, then

$$\mu=N\frac{B_0V}{4\pi}\approx8\ \text{G cm}^3 . \tag{6.9}$$

If one wants to limit $\Omega_{\rm gw}(f)$ to a value of 10^{-10} at 1 kHz or 10^{-9} at 100 Hz, then the magnetic-field spectral density should be less than 10^{-9} G/$\sqrt{\rm Hz}$ at these frequencies.

It is possible that magnetic pushers will not be used in the isolation system for the mass. In this case the dipole moment will most likely result from iron impurities in the mass. Using the worst-case estimate for iron in fused silica, one would have about 50 mg of iron in a 10-kg mass. The magnetic moment for this amount of iron in the Earth's magnetic field would be about 8×10^{-2} G cm^3. This is a factor of 100 less than that for the magnets on the mass. Since the limit on $\Omega_{\rm gw}(f)$ goes as μ^2, the bounds given above will be reduced by 10^{-4}.

The next question is, what is the magnetic-field spectral density that one can expect at a given site? In the frequency regime from the tens of hertz up to a few kilohertz, one sees a somewhat Gaussian background of magnetic-field fluctuations, with a non-Gaussian distribution of burst events superimposed on it. This makes the total probability distribution non-Gaussian. The background is predominantly caused by worldwide lightning events and ionospheric activity, while the bursts are usually due to lightning events within hundreds of kilometers. The background has resonances at certain frequencies, called "Schumann resonances" [31], which are caused by the cavity formed by the Earth and ionosphere.

Ginsberg [32] has measured the magnetic-field fluctuations at Malta and Guam, regions of active magnetic-field activity due to high thunderstorm activity. The value of $B_m(f)\sim4\times10^{-10}$ G/$\sqrt{\rm Hz}$ at 100 Hz was measured at both locations. If one imparts this spectral density onto a full-length–half-length system, then the best limit that one could achieve is $\Omega_{\rm gw}(f)\sim2\times10^{-10}$ at 100 Hz. If the magnetic-field spectral density is as good as was measured in Guam or Malta during their noisiest season, then the correlation between the outputs of the full- and the half-length systems at a single site will not be severely hampered.

A good correlation measurement for $\Omega_{\rm gw}(f)$ may be achieved by two interferometers at a single site in spite of the magnetic-field fluctuations. Therefore a correlation between two interferometers on opposite sides of the continent will surely not be restricted. However, coincident burst events may be registered. A bolt with a peak

current for 10^5 A and at a distance of 2000 km (roughly halfway between interferometers located on the east and west coasts of the U.S.) could produce a noise burst of strain amplitude $h \sim 10^{-22}$, which is very near to the expected sensitivity of the early long-baseline antennas. If one uses the measured event rate for lightning of $2\times10^{-7}/(\text{s km}^2)$, assumes a 500 km by 500 km area in between east and west coasts and the fact that about 2% of the lightning events have a current as large as 10^5 A [33], then, on average, there will be a $h \sim 10^{-22}$ bursts measured simultaneously in both systems every 17 min. These burst will have a total magnetic-field strength of 10^{-4} G at a distance of 2000 km. There is much uncertainty associated with this number. It is likely that the bursts will be concentrated in time around periods of active thunderstorm activity. The magnetic fields will have to be monitored at the interferometer sites so that events can be identified and removed from the data.

Another source of magnetic-field noise that should be addressed is power lines. The power lines leading to an interferometer site will be responsible for providing the necessary megawatt of average power. It is likely that the predominant source of magnetic-field fluctuations will be caused by all the currents in the interferometer facility. The influence on a correlation between a full- and a half-length system at one site will be through the two central masses driven by the same field fluctuation. The tolerable current noise for all the wiring can be found by replacing the spectral density of the field $B_m(f)$ by $I(f)(\text{A}/\sqrt{\text{Hz}})=5B_m(f)r(\text{cm})$, where r should be taken to be about half the distance between the masses. $I(f)$ can then be considered to be the noise from the sum of all the currents in the near vicinity (~ 15 m) in between the two central masses which carry the pusher magnets. At 100 Hz one could limit $\Omega_{\text{gw}}(f)$ to be less than 10^{-8} if $I(f)<12$ $\mu\text{A}/\sqrt{\text{Hz}}$, $\Omega_{\text{gw}}(f)<10^{-9}$ if $I(f)<3.8$ $\mu\text{A}/\sqrt{\text{Hz}}$, or $\Omega_{\text{gw}}(f)<10^{-10}$ if $I(f)1.2$ $\mu\text{A}/\sqrt{\text{Hz}}$. This may prove to be difficult. However, the whole question of magnetically shielding the masses has been omitted. This will undoubtedly improve the situation.

VII. CONCLUSION

In this paper the issue of detecting the SGWB with planned long-baseline laser-interferometric detectors is addressed. There are many potential sources for the SGWB that may be detectable with the systems. The analysis of how one should optimally align two interferometers that are located anywhere on the Earth is presented. This analysis is done so that the probability for detecting the SGWB is maximized. An examination of the correlation experiment involving two or more interferometric detectors is given. The influence of detector orientation and separation on the correlation function is investigated. Optimum filtering and the statistics at correlation are also addressed. The sensitivity of this correlation experiment is calculated. The advanced LIGO system of a 4-km and a 2-km interferometer at one site will be able to limit the energy density of the SGWB to $\Omega_{\text{gw}}(f)<2\times10^{-10}$ at 100 Hz with 10^7 s of integration time. Two 4-km interferometers, separated by 40° of angle of arc around the Earth will be able to attain a limit of $\Omega_{\text{gw}}(f)<6\times10^{-9}$ at 126 Hz. The ultimate LIGO configuration of three full-length and three half-length interferometers at one site and three full-length interfermoters at the other site will be able to constrain the energy density to $\Omega_{\text{gw}}(f)<4\times10^{-11}$ at 100 Hz.

ACKNOWLEDGMENTS

I would like to thank Rainer Weiss, Alan Lightman, Yekta Gürsel, and Massimo Tinto for many useful discussions. This work was supported by NSF Grant No. PHY-8803557.

[1] R. Weiss, in *Sources of Gravitational Radiation,* edited by L. Smarr (Cambridge University Press, Cambridge, England, 1979), p. 7.
[2] R. W. P. Drever, in *Gravitational Radiation,* edited by N. Deruelle and T. Piran (North-Holland, Amsterdam, 1982), p. 321.
[3] K. S. Thorne, in *300 Years of Gravitation,* edited by S. W. Hawking and W. Israel (Cambridge University Press, Cambridge, England, 1987), p. 330.
[4] J. S. Bendat, *Principles and Application of Random Noise Theory* (Wiley, New York, 1958).
[5] T. Vachaspati and A. Vilenkin, Phys. Rev. D **31**, 3052 (1985).
[6] L. P. Grishchuk, Sov. Sci. Rev. E: Astrophys. Space Phys. **7**, 267 (1988).
[7] B. Allen, Phys. Rev. D **37**, 2078 (1988).
[8] V. M. Lipunov, K. A. Postnov, and M. E. Prokhorov, Astron. Astophys. **176**, L1 (1987).
[9] M. Gleiser, Phys. Rev. Lett. **63**, 1199 (1989).
[10] F. R. Bouchet and D. P. Bennett, Phys. Rev. D **41**, 720 (1990).
[11] M. S. Turner and F. Wilczek, Phys. Rev. Lett. **65**, 3080 (1990).
[12] L. P. Grishchuk and A. G Polnarev, in *General Relativity and Gravitation,* edited by A. Held (Plenum, New York, 1980), Vol. 2, p. 393.
[13] R. Weiss, P. Saulson, P. Linsay, and S. Whitecomb, "A Study of a Long Baseline Gravitational Wave Antenna System," MIT report (unpublished).
[14] D. Fattacioli, in *Gravitational Wave Data Analysis,* edited by B. F. Schutz (Kluwer, Dordrecht, 1989).
[15] B. J. Meers, Phys. Rev. D **38**, 2317 (1988).
[16] J. Y. Vinet, J. Phys. (Paris) **47**, 639 (1986).
[17] J. Y. Vinet, B. J. Meers, C. N. Man, and A. Brillet, Phys. Rev. D **38**, 433 (1988).
[18] B. J. Meers, Phys. Lett. A **142**, 465 (1989).
[19] N. Christensen, Ph.D. thesis, MIT, Cambridge, Massachusetts, 1990.
[20] B. F. Schutz and M. Tinto, Mon. Not. R. Astron. Soc. **224**, 131 (1987).
[21] D. Dewey, Ph.D. thesis, MIT, Cambridge, Massachusetts, 1986.
[22] J. C. Livas, Ph.D. thesis, MIT, Cambridge, Massachusetts, 1987.

[23] R. E. Vogt, "A Laser Interferometer Gravitational Wave Observatory (LIGO): Proposal to the National Science Foundation," California Institute of Technology, 1989 (unpublished).
[24] D. F. Morrison, *Multivariate Statistical Methods* (McGraw-Hill, New York, 1976).
[25] R. L. Fante, *Signal Analysis and Estimation: An Introduction* (Wiley, New York, 1988).
[26] P. F. Michelson, Mon. Not. R. Astron. Soc. **227**, 933 (1987).
[27] A. Abramovici, W. E. Althouse, R. W. P. Drever, Y. Gürsel, S. Kawamura, F. J. Raab, D. Shoemaker, L. Sievers, R. E. Spero, K. S. Thorne, R. E. Vogt, R. Weiss, S. E. Whitcomb, and M. E. Zucker, Science **256**, 325 (1992).
[28] G. E. Frantti, Geophysics **28**, 547 (1963).
[29] R. Weiss, report, 1989 (unpublished).
[30] *Corning Glass Works Document on Premium-Quality Fused Silica* (Corning Glass Works, Corning, NY, 1989).
[31] C. Polk, in *CRC Handbook on Atmospherics,* edited by H. Volland (CRC, Boca Raton, FL, 1982), Vol. 1, p. 111.
[32] L. E. Ginsberg, IEEE Trans. Commun. **COM-22**, 452 (1974); **COM-22**, 555 (1974).
[33] R. E. Orville, in *CRC Handbook on Atmospherics* [31], Vol. 2, p. 79.